Journal of Physics B: Atomic, Molecular and Optical Physics

PAPER

Optical isolator based on highly efficient optical pumping of Rb atoms in a miniaturized vapor cell

To cite this article: Eliran Talker *et al* 2020 *J. Phys. B: At. Mol. Opt. Phys.* **53** 045201

IOP Publishing Journal of Physics B: Atomic, Molecular and Optical Physics
J. Phys. B: At. Mol. Opt. Phys. **53** (2020) 045201 (10pp) https://doi.org/10.1088/1361-6455/ab5da7

Optical isolator based on highly efficient optical pumping of Rb atoms in a miniaturized vapor cell

Eliran Talker[1], Pankaj Arora[1], Mark Dikopoltsev[1,2] and Uriel Levy[1]

[1] Department of Applied Physics, The Faculty of Science, The Center for Nanoscience and Nanotechnology, The Hebrew University of Jerusalem, Jerusalem, 91904, Israel
[2] RAFAEL, Science Center, Rafael Ltd, Haifa 31021, Israel

E-mail: ulevy@mail.huji.ac.il

Received 10 October 2018, revised 22 November 2019
Accepted for publication 29 November 2019
Published 24 January 2020

Abstract

We demonstrate both numerically and experimentally the important role of buffer gas in achieving optical isolator based on efficient hyperfine-structure optical pumping of Rubidium (87Rb) atoms in miniaturized vapor cells. It is observed that the increase in the buffer gas pressure allows achieving highly efficient optical pumping. Specifically, at a buffer gas pressure of 40 Torr, it is possible to pump about 85% of the atoms out of the pumped state into the other ground state. While optical pumping has been reported for conventional centimeter-scale cells, we show that in miniaturized cells the role of buffer gas is crucial, as the higher collision rate with the walls diminishes the effect of optical pumping, posing a stringent limitation on the applicability of optical pumping in miniaturized systems. Following the results reported herein, we demonstrate an optical isolator with isolation ratio better than 20 dB at a relatively low temperature of about 80 °C, and with a low magnetic field (~800 Gauss). The obtained results provide another step forward in the quest for miniaturizing quantum devices. The demonstrated device shows that such miniaturized vapor cells can be considered for applications such as all-optical switching, optical quantum memory, frequency references, and magnetometry to name a few.

Supplementary material for this article is available online

Keywords: light-matter interaction, atom optics, optical pumping, quantum description of light-matter interaction, optical isolator

(Some figures may appear in colour only in the online journal)

Introduction

Optical pumping is a powerful technique to create and maintain a non-equilibrium state of populations of atoms in different quantum states by means of resonant absorption of light [1, 2]. These states can be of different fine-structure levels [2], different Zeeman sublevels [3] or different hyperfine-structure levels [4]. The population exchange of atoms across the different states can be monitored by the measured intensity or polarization of the scattered resonance light or by the change in light transmission through the cell [5, 6].

Optical pumping has been used quite often to exchange the population of atoms in Zeeman sublevels of the ground state [1, 3, 7]. Furthermore, it was shown that strong population differences between hyperfine levels can be achieved by optical pumping techniques, without the use of a magnetic field [4, 8, 9]. In optical pumping of pure Rb atoms (i.e. without the presence of buffer gas), the mean free time (defined as the average collision time of the Rb atom with the cell walls) can be shorter than the life-time of the excited state. As a result of which, the atoms which collide with the walls of the cell, suppress the optical pumping efficiency

since collision causes the atoms to lose their spin coherence. By losing their spin memory, the atoms return back to one of the two ground states according to Boltzmann distribution.

In order to preserve the spin-polarized ground state of atoms in a vapor cell, the use of anti-relaxation coatings such as Paraffin has been reported to improve optical pumping [10–13]. While the use of anti-relaxation coatings is a promising approach, it has also some disadvantages, e.g. the low melting point of the material used for the coating [14]. The realization of such coatings may also be challenging from the technological point of view.

As an alternative, the use of inert buffer gas, typically a noble gas such as argon, or neon or inert gases such as nitrogen in a vapor cell has been studied to improve optical pumping [8, 15, 16]. Though the use of buffer gas causes pressure broadening in the optical transition, still, it allows keeping the atoms in interaction with the optical beam for a much longer time. As compared with anti-relaxation coatings, buffer gas allows working at elevated temperatures [17]. The collisions of atoms with the buffer gas reduce the probability of the optically spin oriented atoms to reach the wall, where they lose their spin orientation. If the gas density is sufficiently high, the mean free path of the atoms becomes small as their motion is governed by a slow diffusion process in a gas environment (instead of ballistic motion in the absence of buffer gas) which helps to achieve efficient optical pumping [15, 18, 19].

In parallel to these efforts, we are witnessing significant efforts towards the miniaturization of vapor cells to a millimeter scale and even below, with the final goal of enabling efficient and compact chip-scale light-vapor interactions [20–26]. Laser spectroscopy employing miniaturized vapor cells is attracting growing attention, primarily for its potential applications in compact frequency standards [27], magnetometry [28, 29], and optical isolator [30]. Optical isolators, which allow the transmission of light in only one direction, are the basic optical components for many laser systems since they prevent unwanted feedback resulting in a number of instabilities [31].

Yet, miniaturization of cells brings about the penalty of increasing the collision rate of atoms with the wall of the cell as compared to the conventional vapor cell. As such, it is far more challenging to achieve optical pumping in miniaturized cells as compared to conventional Rb cells (see supporting information). Thus, the role of buffer gas is expected to become crucial in achieving optical pumping with such cells. Achieving optical pumping in such miniaturized vapor cells using buffer gas to demonstrate a relatively low temperature ($\sim$80 °C) optical isolator is the topic of our current paper.

In this paper, we start by exploring theoretically and experimentally light-vapor interactions in miniaturized (Length = 1 mm, Radius = 0.5 mm) vapor cell in the presence of buffer gas. Specifically, we investigate the first efficient hyperfine optical pumping of 87Rb atoms in a miniaturized vapor cell filled with buffer gas of different pressures. The mechanism for population exchange of 87Rb atoms in our cells is studied theoretically using a density matrix approach and verified experimentally. We observed that the increase in buffer gas pressure (we use a {2: 1} mixture of N_2 and Ar in order to minimize the shift in energy levels) in the cell under a pump-probe scheme allows achieving efficient optical pumping. Finally, we demonstrate the usefulness of achieving efficient optical pumping with buffer gas, by demonstrating an optical isolator under the pump-probe beam scheme in a miniaturized vapor cell.

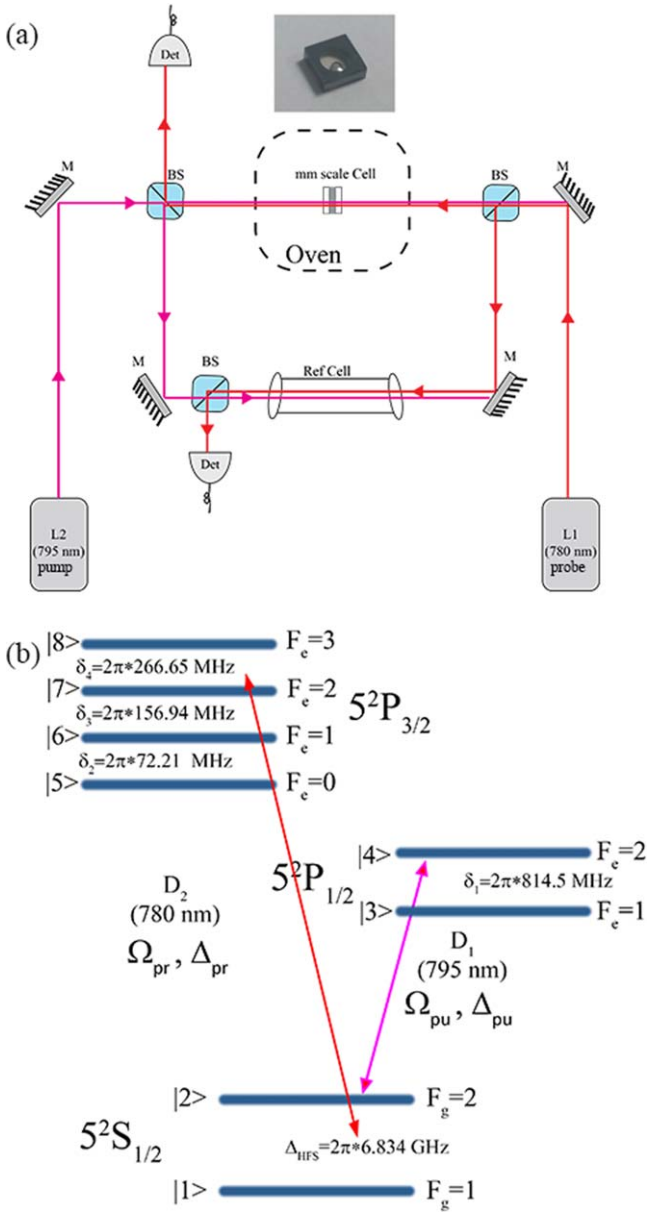

Figure 1. (a) Schematic of the experimental setup for optical pumping. M: Mirror, BS: Beam Splitter, Det: Photodetector. (b) Scheme of 87Rb energy levels showing the D_1 and D_2 lines related to the optical pumping process.

Experimental setup

Figure 1(a) shows a sketch of our experimental setup including a photograph of our miniaturized vapor cell which is used to achieve hyperfine optical pumping under a pump-probe scheme. The beam from 795 nm laser L2 (Toptica DL100) with a $1/e^2$

beam radius of 0.5 mm is acting as a strong pump beam while the beam from 780 nm laser L1 (Toptica DL pro), also with a $1/e^2$ beam radius 0.5 mm is acting as a weak probe beam. The pump and probe beams pass through the miniaturized vapor cell filled with 87Rb. A counter propagation beam configuration was used to ease the separation of the pump and the probe beam. Several different cells with different levels of buffer gas pressure are used. Beam splitters and mirrors are used to tap some of the light from both laser beams into a 7.5 cm long pure isotope Rb reference cell. The reference cell is used in the experiment to ensure that both pump and probe beams are coupled to desired transition levels. Photodetectors (Thorlabs Det100) are used to capture the 780 nm probe beam transmitted through the cells. The intensity for both the pump and probe beam is controlled by neutral density filters. All the measurements are done at a temperature of 40 °C using a homemade resistive oven. The miniaturized vapor cells are created by the process of anodic bonding in a glove box environment. The fabrication process of such cells is closely resembling the description which was published in [32]. To prevent spontaneous decay, a quenching gas, typically a diatomic molecule such as N_2, is added to the cell. In the presence of N_2, the absorption line will be positively frequency shifted (Blue-shift), because of collisions of the Rb atoms with the buffer gas. Ar, on the other hand, results in a negative frequency shift (Red-shift). In order to compensate for the shift, we use a mixture of N_2 and Ar with a ratio of 2:1. The choice of these two types of buffer gases is a standard way to reduce the frequency shift. In this case, the frequency shift $\Delta\nu_{bg}$ can be approximated in a limited temperature as [33]

$$\Delta\nu_{bg} = P[(r_1\beta_1 + r_2\beta_2) + (r_1\psi_1 + r_2\psi_2)(T - T_0) + (r_1\varsigma_1 + r_2\varsigma_2)(T - T_0)^2], \quad (1)$$

where β_i, ψ_i and ς_i with $i = 1, 2$ are the pressure and temperature coefficients for buffer gas 1, 2 respectively. r_1 and r_2 denote the ratio between the buffer gas pressure for the buffer gas, 1 and 2 respectively such that $r_1 + r_2 = 1$. P is the total pressure of the buffer gas and T is the temperature in Kelvin.

Figure 1(b) shows the scheme for an eight-level atomic system of 87Rb considered as two ground levels $|1\rangle$, $|2\rangle$ which are related to the hyperfine levels $F_g = 1, 2$ respectively. The levels $|3\rangle$, $|4\rangle$ are the levels of the D_1 transition, which are separated by $2\pi^*814.5$ MHz. The other four levels ($|5\rangle$, $|6\rangle$, $|7\rangle$, $|8\rangle$) are related to the D_2 transition with different level spacing as shown in figure 1(b). This system interacts with the counter-propagating pump and probe beams, where the pump beam (795 nm) is aligned with the D_1 transition and the probe beam (780 nm) is aligned with the D_2 transition. The Δ_{pr}, Δ_{pu} are the linear detuning and Ω_{pr}, Ω_{pu} are the Rabi frequencies of the probe and pump beam respectively.

Numerical results

In order to understand the mechanism of optical pumping, we have plotted the real part of the density matrix (ρ) in steady-state (i.e. $\rho_{ij} = |i\rangle\langle j|$) as shown in figure 2 (see supporting information is available online at stacks.iop.org/JPB/53/045201/mmedia for density matrix approach). The obtained results for different pressure values of buffer gas are shown in figures 2(a)–(d). We can clearly see that by setting the pump laser beam to the transition of $F_g = 2$ to $F_e = 1, 2$ (D_1 transition), the efficiency of optical pumping is increasing with the increase of buffer gas pressure. Specifically, at a pressure of 40 Torr, it is possible to pump about 85% of the atoms out of the pumped state into the other ground state as shown in figure 2(d). The populations of the ground states ($F_g = 1$ and $F_g = 2$) are obtained from the elements ρ_{11} and ρ_{22} respectively. Here, the presence of the buffer gas increases the interaction time of the atoms with the optical beam due to the higher collision rate with a buffer gas. As such, the spin states are maintained for a longer time, which is sufficiently long to allow efficient optical pumping.

Figure 3 shows the simulated steady-state imaginary part of the susceptibility as a function of the linear probe detuning, considering a vapor cell filled with buffer gas of different pressure values. The susceptibility χ describes the degree of polarization of a dielectric medium in response to an electric field. The imaginary part of the optical susceptibility $\chi_I(\Delta_{pr})$ is derived from the density matrix of the eight-level atomic system. Taking into account the selection rules, the imaginary susceptibility terms are calculated by

$$\chi_I(\Delta_{pr}) = -\frac{2N}{\epsilon_0\hbar\Omega_{pr}}\left(\mathrm{Im}\sum_{i=6}^{8} d_{2,i}^2\rho_{2,i}(\Delta_{pr}) + \mathrm{Im}\sum_{i=5}^{7} d_{1,i}^2\rho_{1,i}(\Delta_{pr})\right), \quad (2)$$

where N is the uniform number density for an atomic ensemble and d represents the dipole matrix.

The blue curve shows the calculated absorption spectrum taking into account the natural lifetime, whereas the red curve predicts the total line width by also including the effect of residual Doppler broadening (due to the difference in wavelength between pump and probe) and pressure broadening. In figure 3(a), we show the imaginary susceptibility curve for the case where no buffer gas is present. As can be observed, the effect of optical pumping is negligible. This is due to the high rate of collisions with the walls. Figures 3(b)–(d) represent the scenario of increasing buffer gas pressure. As a result, the effect of optical pumping becomes more noticeable as manifested by the increase in susceptibility of the transitions aligned with the $F_g = 1$ level and the decrease in susceptibility of the transitions aligned with the $F_g = 2$ level. For small values of buffer gas pressure, the wall collision rate is still higher than the lifetime of the excited state and therefore most of the atoms still lose their coherence and therefore occupied each of the ground states with equal probability, which reduces the optical pumping efficiency. On the other hand, with the increase of the buffer gas pressure, we could also see the increase in optical pumping efficiency. This, however, is followed by linewidth broadening due to pressure broadening mechanism. Indeed, the hyperfine transitions, which are well separated for the case of low buffer gas pressure, become un-noticeable for larger gas pressures. All

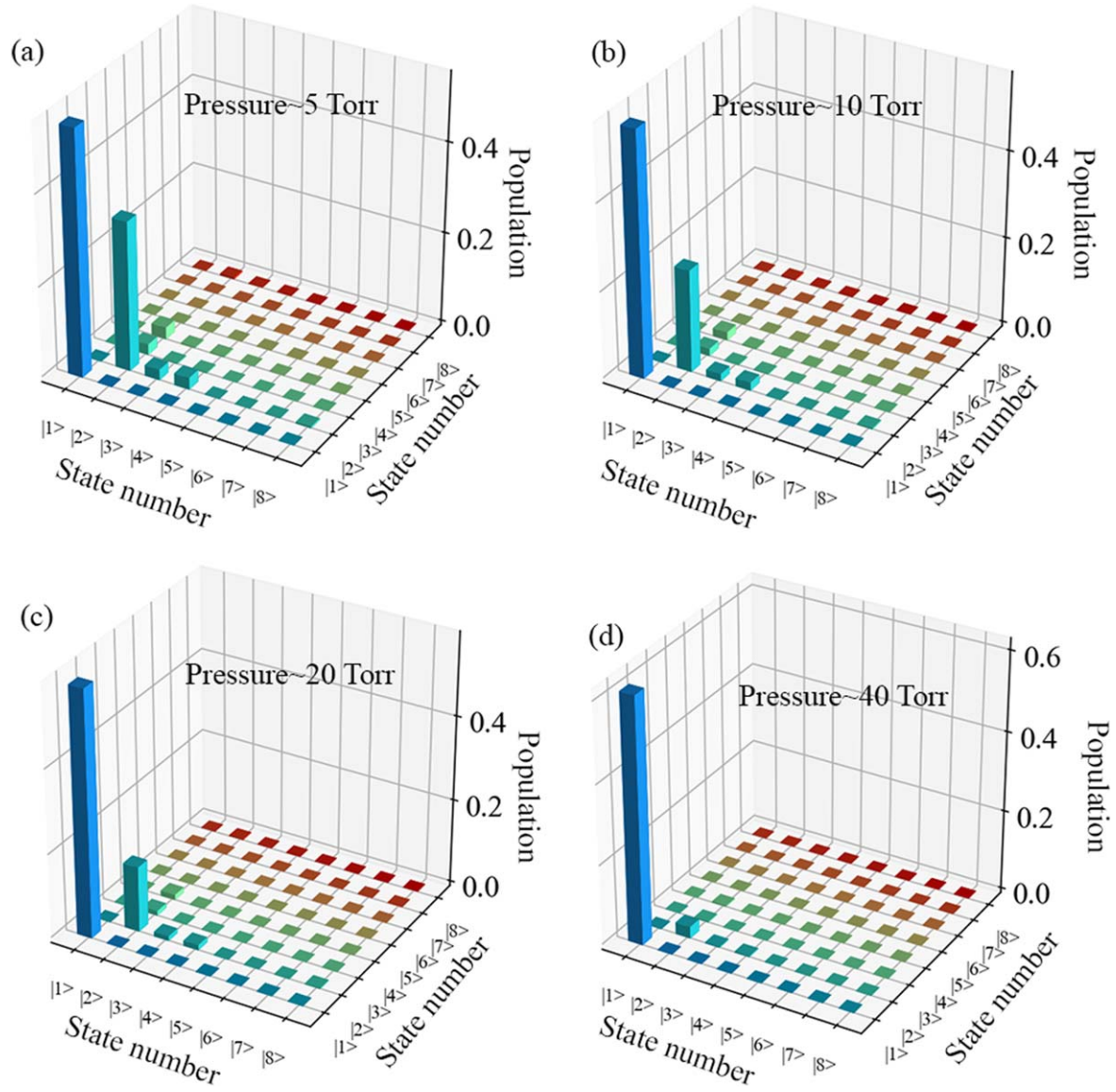

Figure 2. Simulated density matrix elements achieved by optical pumping with pressure values of (a) 5 Torr (b) 10 Torr (c) 20 Torr (d) 40 Torr respectively.

the simulations were carried out assuming a temperature (T) of 40 °C while setting Rabi frequency of the pump to Ωpu $= 10.\Gamma_1$, and the probe Rabi frequency to $\Omega_{pr} = \Gamma_2$ where $\Gamma_1 = 2\pi \cdot 5.75$ MHz corresponds to the D_1 transition, and $\Gamma_2 = 2\pi \cdot 6.06$ MHz corresponds to the D_2 transition respectively.

In figure 4, we show the simulated transmission curve (dashed black) without and with optical pumping for buffer gas pressure of 40 Torr corresponding to levels $F_g = 1$ and 2 respectively. When the pump beam is applied (figure 4(b)), optical pumping is achieved due to increase in the population of the atoms at level $F_g = 1$, whereas in the absence of the pump beam (figure 4(a)), both the dips corresponding to $F_g = 1$ and $F_g = 2$ are observed to have almost the same contrast (the contrast defined as $\frac{|S_H - S_L|}{|S_H + S_L|}$ where $S_{H,L}$ stands for the highest and lowest value of the signal, respectively).

Experimental results

Next, we turned into the experimental observation of optical pumping in our vapor cells filled with a buffer gas. Using the same scheme as described in figure 1(a), the transmission of the probe beam (780 nm) with and without optical pumping through the vapor cell having buffer gas pressure of around 40 Torr is measured as shown in figure 4(solid red). For a pump power of 2.5 mW and probe power of 15 μW, efficient optical pumping features (figure 4(b)) are clearly observed. In the absence of the pump beam (figure 4(a)), the contrast of the $F_g = 1$ transition is significantly reduced, whereas the contrast of the $F_g = 2$ reaches the value of about 1%, in agreement with the simulated results.

To confirm the effect of buffer gas pressure on the optical pumping as described above, we measured the transmission of the probe beam through several vapor cells filled with

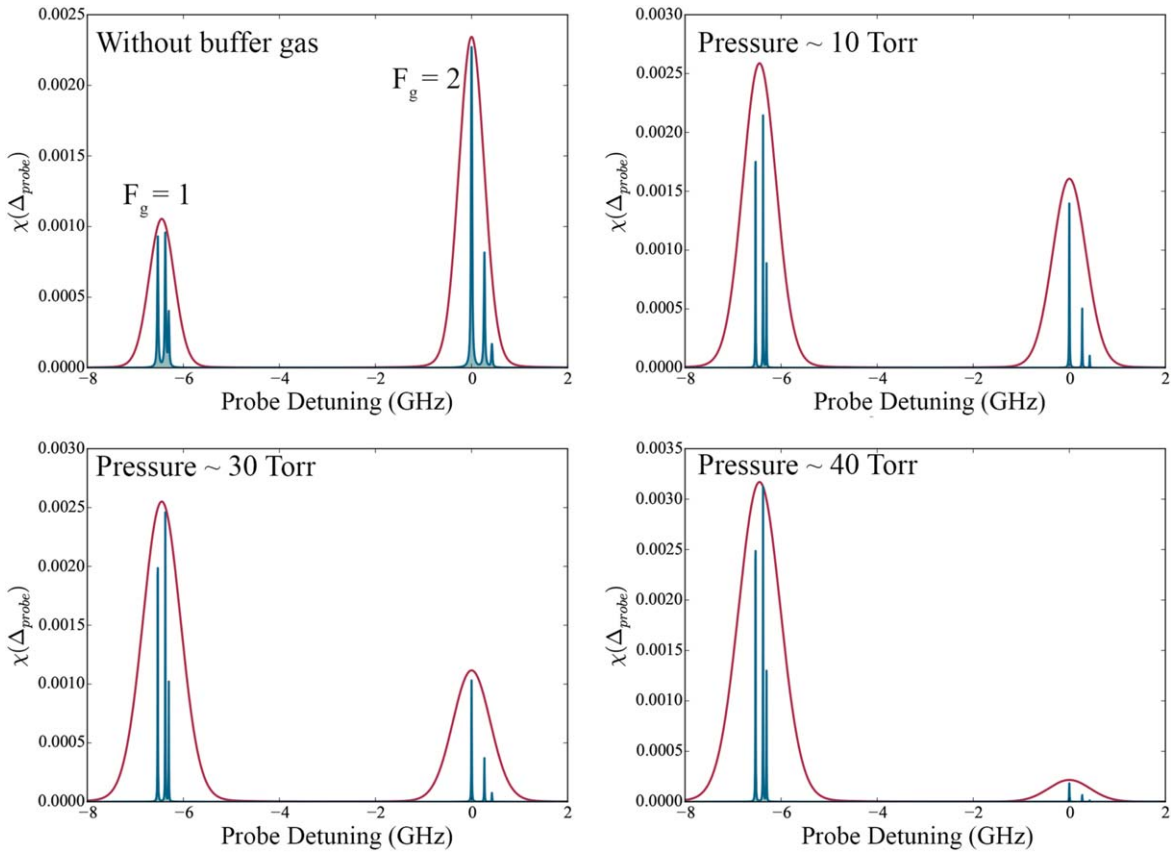

Figure 3. Simulated normalized steady-state imaginary susceptibility as a function of the linear probe detuning for pressure values of (a) 0 (i.e. without buffer gas), (b) 10 Torr, (c) 30 Torr, and (d) 40 Torr. Blue—natural linewidth only. Red—including the effect of residual Doppler broadening and pressure broadening.

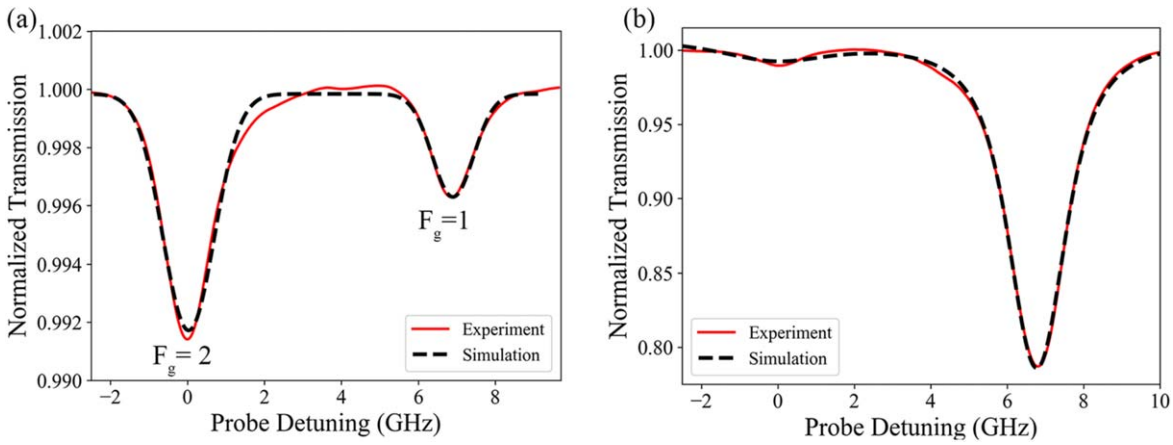

Figure 4. Experimental (solid red) and simulated (dashed black) transmission curves for our miniaturized vapor cell with buffer gas pressure of ∼40 Torr (a) without and (b) with optical pumping respectively. $L = 1$ mm, $R = 0.5$ mm, $T = 40$ °C and probe intensity of 15 μW and pump intensity of 2.5 mW.

buffer gas of different pressure values as shown in figure 5. We can clearly observe that with a gradual increase in the pressure of the buffer gas, the effect of optical pumping becomes more noticeable. In parallel, one can also notice the increase in pressure broadening with the increase in buffer gas pressure. As such, enhanced optical pumping is accompanied by a broader line width of transition. This can be favorable for applications such as all-optical switching [20], where bandwidth is important. On the other hand, such broadening is less desired for applications such as magnetometry [28].

Then, we studied the effect of pump beam intensity on optical pumping, by measuring the transmission of the probe beam through our miniaturized vapor cell with buffer gas pressure of 40 Torr. Figure 6(a) shows the simulated transmission curve for different values of pump beam Rabi frequencies whereas the Rabi frequency of the probe beam was

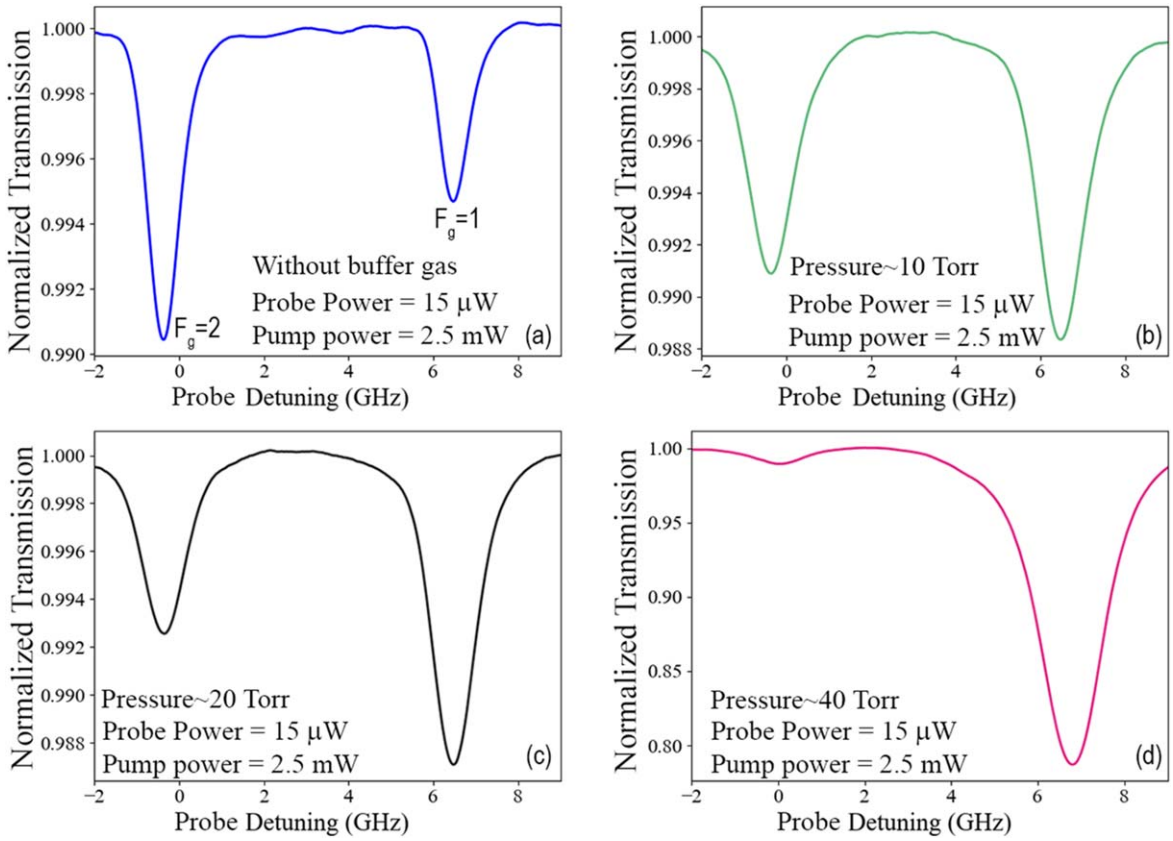

Figure 5. Experimentally obtained transmission curves in miniaturized vapor cell for different buffer gas pressure of (a) 0 Torr {without buffer gas}, (b) 10 Torr, (c) 20 Torr, and (d) 40 Torr respectively.

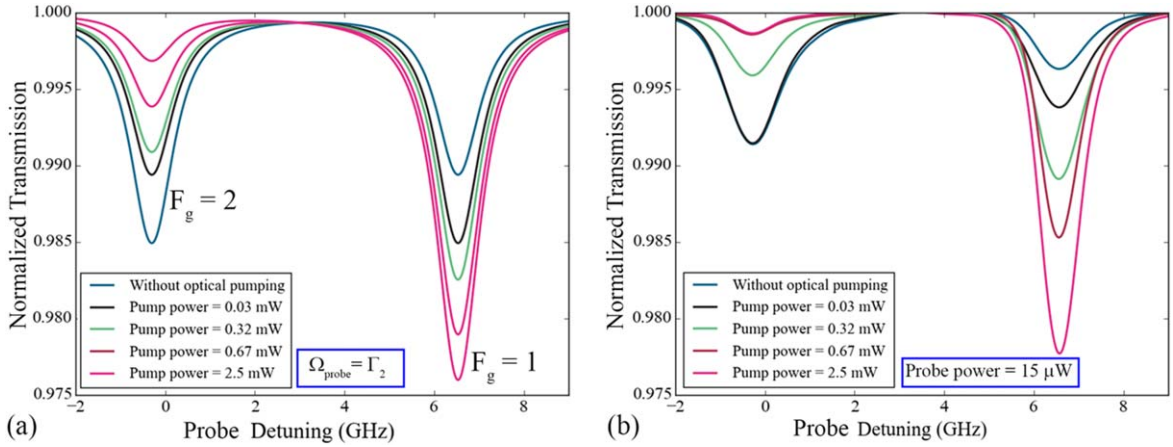

Figure 6. (a) Simulated and (b) experimentally measured transmission curves in miniaturized vapor cell with buffer gas pressure of around 40 Torr with variation in pump power.

kept constant. With the increase in the pump beam Rabi frequency (i.e. power), the increase in the contrast of the optical pumping can be clearly observed. To verify the simulation results, the transmission curves for the same vapor cell were experimentally measured with different power values of the pump beam as shown in figure 6(b). The probe power during this experiment was kept to be constant (15 μw). Similar to the simulation results, the same features of enhanced optical pumping with the increase in pump power could be clearly observed in the measured transmission curves. As can be seen, highly efficient optical pumping was obtained.

Realization of an optical isolator

Optical isolators are fundamental components in a variety of optical systems, typically used for the purpose of blocking backscattered light from arriving into the laser. By doing so, undesired effects such as laser instabilities and mode hopping

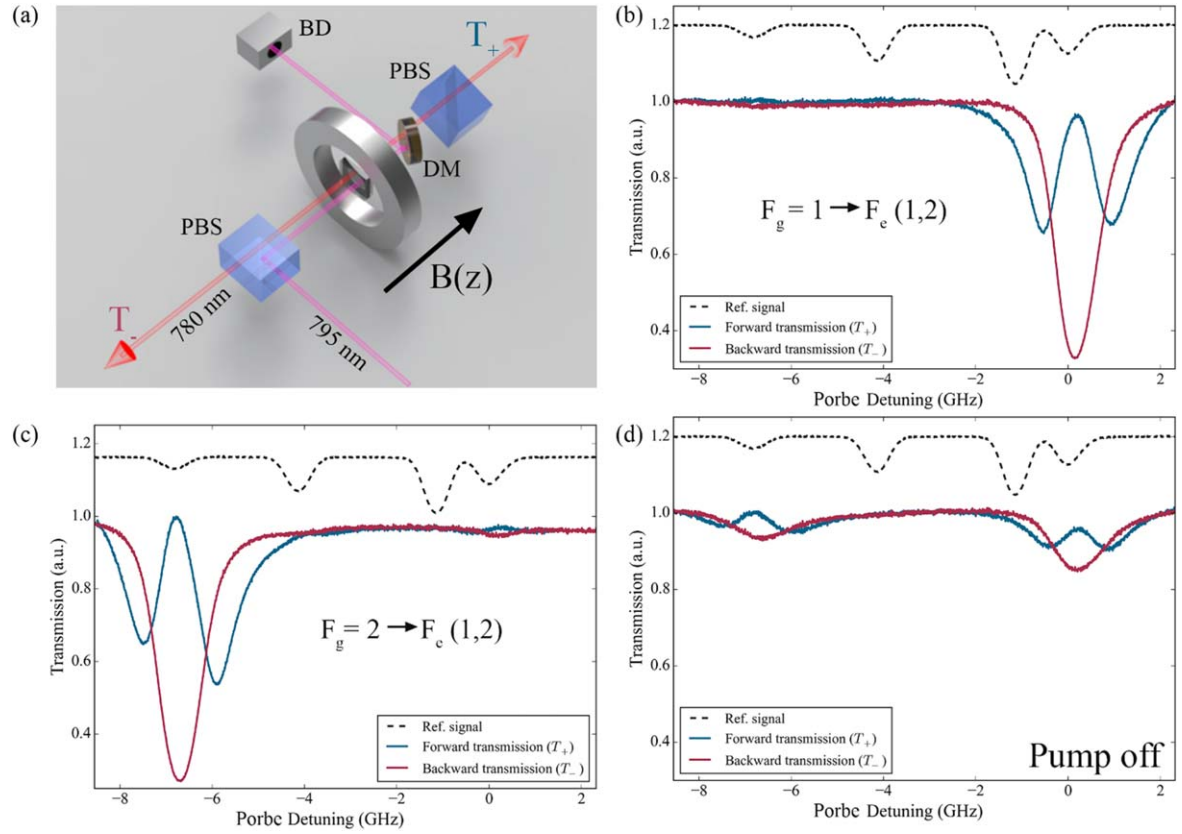

Figure 7. (a) Experimental set up to realize an optical isolator in a miniaturized vapor cell; PBS: Polarization Beam Splitter, DM: Dichroic Mirror, BD: Beam Dump. (b), (c) Forward $\boldsymbol{T}_+$ (blue) and backward $\boldsymbol{T}_-$ (red) transmission as a function of linear probe detuning, demonstrating the optical isolator effect by locking the pump beam to (b) $\boldsymbol{F_g} = 1$ and (b) $\boldsymbol{F_g} = 2$ respectively. All the measurements were taken at 60 °C using a cell with a buffer gas pressure of 40 Torr. (d) Forward (blue) $\boldsymbol{T}_+$ and backward (red) $\boldsymbol{T}_-$ transmission as a function of the linear probe detuning when the pump beam is off.

are significantly suppressed. The basic principle of an optical isolator relies on the Faraday effect. In more detail, one may consider an atomic vapor cell, placed between two crossed linear polarizers, or polarized beam splitters (figure 7(a)). When an external magnetic field is applied along the optical axis, the m_{F} levels split in an asymmetric manner. The σ^+ and σ^- components of the linearly polarized light, now experience different phase shifts when passing through the medium, this results in a net rotation of the linearly polarized light. Using the principle of the Faraday effect as shown in figure 7(a), a beam passes through the cell where the magnetic field is applied parallel to the optical axis. A second PBS is rotated by $\pi/4$ with respect to the first one, allowing high transmission along the positive z-direction (T_+) for an induced polarization rotation of $\pi/4$. With this arrangement, one would also expect isolation along the negative z-direction (T_-). An ideal isolator provides a $\pi/4$ polarization rotation alongside with minimal absorption. The angle of rotation is given by

$$\theta \approx N \cdot Po \cdot L, \tag{3}$$

where L is the path length of the probe beam through the cell, N is the density of alkali atoms, and Po is the polarization of the alkali vapor along the probe beam direction (for more details see the supporting information). As can be seen from equation (3), increasing the density and/or the polarization will increase the Faraday rotation. The density can be increased by increasing the operating temperature. However, increasing the temperature will also increase the undesired absorption and will broaden the optical linewidth. The polarization is increased by applying a strong magnetic field. In such a case, the thermal polarization is given by [34]

$$Po_{thermal} = \tanh\left(\frac{\frac{1}{2} g_s \mu_B B}{k_B T}\right), \tag{4}$$

where $g_s \approx 2$ is the electron g-factor and $\mu_B = 2.97 \times 10^{-24}$ J T^{-1} is the Bohr magneton constant, k_B is the Boltzmann constant and B is the magnetic field. For example, at the temperature of 80 °C, a very strong magnetic field of about 10 T is needed to achieve a relatively low polarization factor of ~0.01.

Alternatively, one may consider operating in the nonequilibrium regime by using optical pumping. Optical pumping increases the polarization by changing the population of atoms from one m_{F} level of a ground state to another m_{F} level of a ground state level via an excited state. Large nonthermal spin polarization, with $Po \sim 1$ can be obtained by optical pumping, which transfers the angular momentum from resonant light to the atoms (see supplementary information). Here, we take advantage of this approach to demonstrate optical

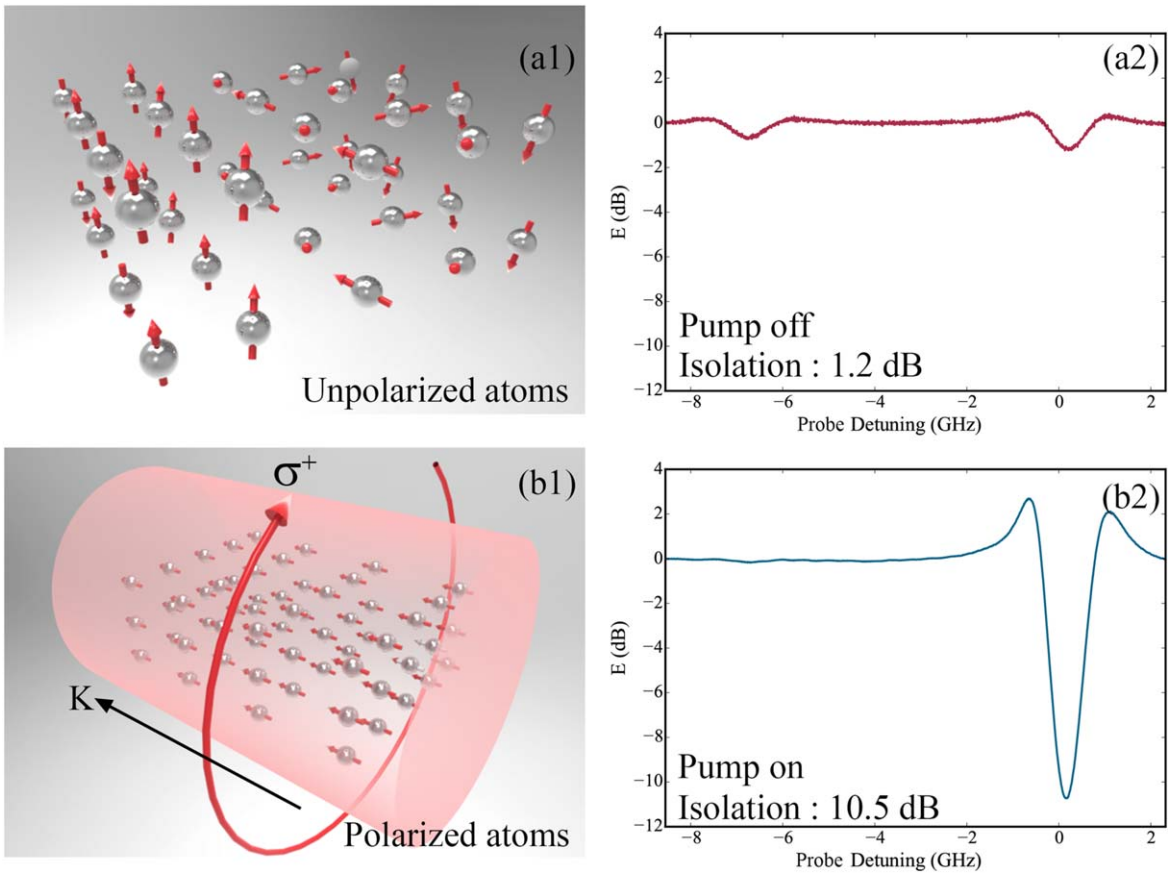

Figure 8. Optically pumped and unpumped optical isolator principle of operation: (a1) The rubidium atoms of the vapor cell have randomly oriented atomic spins (a2) Optical isolator effect as a function of linear probe detuning without pump beam. (b1) Using circularly polarized pump laser (795 nm), the spins are aligned in the propagation direction of the pump laser. (b2) Optical isolator effect as a function of probe detuning with the pump beam.

isolation in our miniaturized vapor cell. Due to the non-thermal polarization, we can achieve a high isolation ratio better than 20 dB at a temperature of about 80 °C and with the low magnetic field of about 800 Gauss. Both the temperature and the field values are significantly lower than the values used in [30].

The experimental setup is shown in figure 7(a). The measurements are taken at a temperature of 60 °C in order to increase the optical density and hence increasing the optical isolator efficiency. The σ^+ polarized pump light ($\lambda = 795$ nm, pink color) is used to pump the atoms and is later filtered out using Dichroic Mirror (DM) and sent to a Beam Dump (BD). The probe beam ($\lambda = 780$ nm, red color) is linearly polarized along the horizontal direction using Polarization Beam Splitter (PBS). Figures 7(b)–(d) show the transmission as a function of the probe beam detuning. Figure 7(b) shows the transmission when the pump beam is fixed to $F_g = 1 \rightarrow F_e = 1, 2$ while figure 7(c) shows the transmission when the pump beam is fixed at $F_g = 2 \rightarrow F_e = 1, 2$. From figures 7(b), (c), one clearly observes the isolation effect. Furthermore, the frequency operation of our isolator can be switched between two values separated by ∼6.8 GHz. Simply by tuning the pump beam to each of the two ground states ($F_g = 1$ and $F_g = 2$) of 87Rb as shown in figures 7(b) and (c) respectively, the frequency of the probe in which isolation occurs is shifted by about 6.83 GHz, in correspondence with the separation between the two ground states. As a control experiment (figure 7(d)), we have repeated the measurement, this time when turning off the pump beam. As can be seen, for such a case the transmission in both directions is nearly identical. In other words, by switching the pump beam on and off, we are able to switch the optical isolator on and off.

To further investigate the performance of our realized optical isolator, we define the isolation of the device as $E = -10\log(T_+/T\_)$ (dB). The isolation for the cases where the pump is off and on is now presented in figure 8, alongside with a schematic illustration showing the polarization of the atoms. Figure 8(a1) presents a schematic illustration showing the random direction of the atoms for the case where the pump is off. For such a case, the maximal isolation is about 1.2 dB with the transmission of around 20% (figure 8(a2)). In contrast, when the pump beam is on, the atoms are oriented in the same direction (figure 8(b1)). For such a case, the isolation reaches a value of ∼10 dB with ∼ 90% transmission (figure 8(b2)).

Next, we test the isolation for different values of buffer gas pressure. As shown in figures 9(a), (c), for 20 Torr buffer gas pressure, the obtained transmission is ∼80% (figure 9(a)) and the isolation is nearly 7 dB (figure 9(c)). By increasing the buffer gas pressure to 40 Torr (figures 9(b), (d)), the

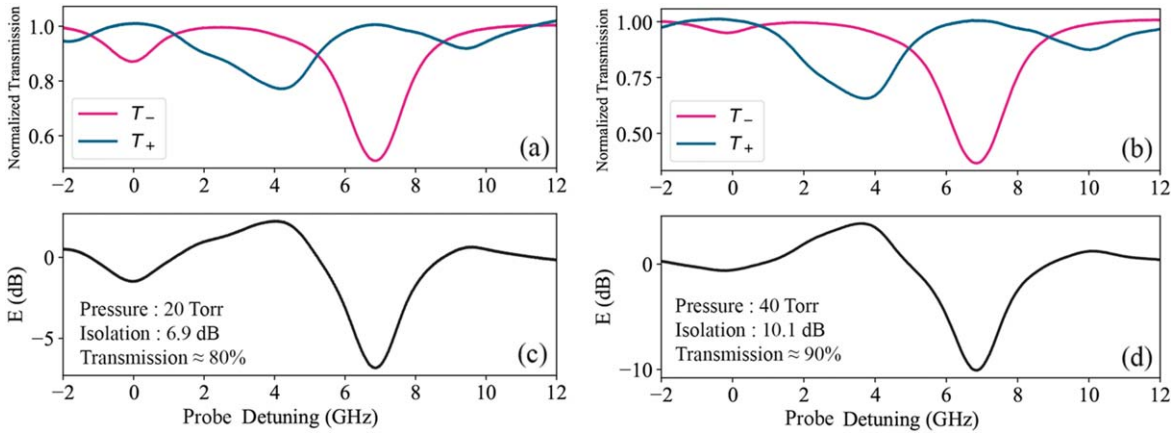

Figure 9. Isolator effect as a function of linear probe detuning with buffer gas pressure of (a), (c) = 20 Torr (b), (d) = 40 Torr respectively. The operating temperature is 60 °C with a magnetic field of 800 G. The pump beam is fixed to $F_g = 1 \rightarrow F_e = 1, 2$.

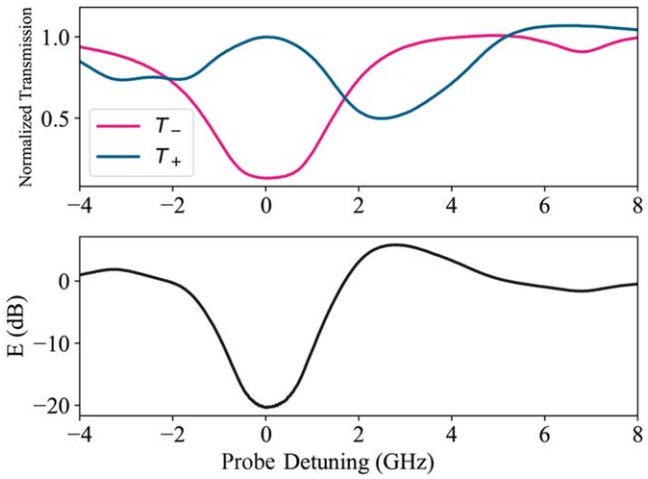

Figure 10. (a) Transmission for forward and backward propagating beam and (b) isolation as a function of linear probe detuning for 40 torr buffer gas pressure; with operating temperature of 80°C and magnetic field of 800 G.

transmission is increased to ∼90% (figure 9(b)), whereas the isolation reaches the value of 10 dB (figure 9(d)). The reason for the increase of the isolation is that the polarization value (see supplementary information) for 40 Torr is larger than the polarization value for the 20 Torr.

Finally, we demonstrate the increase in isolation efficiency by increasing the temperature to around 80 °C as shown in figure 10. As we can see, the isolation is about to 20 dB, while the transmission of the forward beam is about the same as in the previous case (figure 10(b)). The isolation can be further improved by increasing the temperature of the cell or by increasing the strength of the magnetic field as was done in [30].

Conclusions

We have demonstrated the importance of buffer gas in achieving efficient optical pumping of 87Rb atoms in miniaturized vapor cells. When buffer gas is not present, the rubidium atoms take a ballistic trajectory and quickly collide with the walls of the cell. Given the small dimensions of the cell, the high collision rate is faster than the lifetime of the excited state. As a result, such collisions do not allow for efficient optical pumping to occur. However, with the presence of buffer gas, the motion of the atoms become diffusive-like, and the collision rate is significantly reduced, giving rise to an efficient optical pumping even in miniaturized cells. The mechanism of the hyperfine-structure based optical pumping was studied theoretically by considering eight levels atomic system of the 87Rb scheme using a density matrix approach, followed by experimental characterization of the transmission of the probe beam through the miniaturized vapor cell. The numerical and experimental results indicated that indeed the efficiency of optical pumping is enhanced with the increase in buffer gas pressure within the vapor cell. Finally, this efficient optical pumping scheme is used to demonstrate an optical isolator with the transmission of about 90% and isolation of about 20 dB using a reasonable temperature of 80°C with the magnetic field as low as 800 G. The operation frequency of the isolator can be switched in frequency by 6.8 GHz by switching the frequency of the pump beam.

The obtained results provide significant progress in the quest for miniaturizing quantum devices. The buffer gas-filled miniaturized cell can be used in applications such as all-optical switching, optical quantum memory, frequency references, and magnetometry to name a few. Future work will be devoted to the study and the demonstration of such optical pumping effects in even more miniaturized cells, down to the micro and the nanoscale level.

Acknowledgments

We acknowledge financial support from the ERC project Light-Vapor-Interactions on a chip (LIVIN) and the Israeli Science Foundation (ISF). We thank Rafael Advanced Defense Systems (Israel) for the preparation of buffer gas-filled 87Rb vapor cells.

ORCID iDs

Eliran Talker https://orcid.org/0000-0001-7182-9762
Pankaj Arora https://orcid.org/0000-0002-0451-9518

References

[1] Happer W 1972 Optical pumping *Rev. Mod. Phys.* **44** 169–250
[2] Bergmann K, Theuer H and Shore B W 1998 Coherent population transfer among quantum states of atoms and molecules *Rev. Mod. Phys.* **70** 1003–23
[3] Dancheva Y, Alzetta G, Cartaleva S, Taslakov M and Andreeva C 2000 Coherent effects on the Zeeman sublevels of hyperfine states in optical pumping of Rb by monomode diode laser *Opt. Commun.* **178** 103–10
[4] Cruzeiro E Z, Tiranov A, Lavoie J, Ferrier A, Goldner P, Gisin N and Afzelius M 2018 Efficient optical pumping using hyperfine levels in Nd^{3+}: Y_2SiO_5 and its application to optical storage *New J. Phys.* **20** 053013
[5] Lindvall T 2010 *Alkali-Metal Atoms in Laser Fields : Optical Pumping, Coherent Population Trapping, and Laser Cooling* Aalto University
[6] Cohen-Tannoudji C and Kastler A 1966 *Optical Pumping* (Amsterdam: North-Holland)
[7] Kastler A 1957 Optical methods of atomic orientation and of magnetic resonance *J. Opt. Soc. Am.* **47** 460–5
[8] Moretti A and Strumia F 1971 Hyperfine optical pumping of sodium vapors *Phys. Rev.* A **3** 349–54
[9] Smith D A and Hughes I G 2004 The role of hyperfine pumping in multilevel systems exhibiting saturated absorption *Am. J. Phys.* **72** 631–7
[10] Klein M, Novikova I, Phillips D F and Walsworth R L 2006 Slow light in paraffin-coated Rb vapor cells *J. Mod. Opt.* **53** 2583–91
[11] Balabas M V, Jensen K, Wasilewski W, Krauter H, Madsen L S, Müller J H, Fernholz T and Polzik E S 2010 High-quality anti-relaxation coating material for alkali atom vapor cells *Opt. Express* **18** 5825–30
[12] Balabas M V, Karuzin M I and Pazgalev A S 1999 Experimental investigation of the longitudinal relaxation time of electronic polarization of the ground state of potassium atoms in a cell with an antirelaxation coating on the walls *J. Exp. Theor. Phys. Lett.* **70** 196–200
[13] Bouchiat M A and Brossel J 1966 Relaxation of optically pumped Rb atoms on paraffin-coated walls *Phys. Rev.* **147** 41–54
[14] Li W, Peng X, Budker D, Wickenbrock A, Pang B, Zhang R and Guo H 2017 Hybrid optical pumping of K and Rb atoms in a paraffin coated vapor cell *Opt. Lett.* **42** 4163–6
[15] Larson B, Häusser O, Delheij P, Whittal D and Thiessen D 1991 Optical pumping of Rb in the presence of high-pressure ^{3}He buffer gas *Phys. Rev.* A **44** 3108–18
[16] Arditi M and Carver T R 1964 Hyperfine relaxation of optically pumped Rb87 atoms in buffer gases *Phys. Rev.* **136** A643–9
[17] Appelt S, Baranga A B A, Young A R and Happer W 1999 Light narrowing of rubidium magnetic-resonance lines in high-pressure optical-pumping cells *Phys. Rev.* A **59** 2078–84
[18] Erhard M and Helm H 2001 Buffer-gas effects on dark resonances: theory and experiment *Phys. Rev.* A **63** 1–13
[19] Hu Z F, Du C G and Wang Y Z 2006 Buffer-gas-induced narrowing of electromagnetically induced transparent spectra for an open system *Journal of Modern Optics* 53 **4** 513–23
[20] Stern L, Grajower M and Levy U 2014 Fano resonances and all-optical switching in a resonantly coupled plasmonic–atomic system *Nat. Commun.* **5** 1–9
[21] Stern L, Desiatov B, Mazurski N and Levy U 2017 Strong coupling and high-contrast all-optical modulation in atomic cladding waveguides *Nat. Commun.* **8** 1–7
[22] Yang W, Conkey D B, Wu B I N, Yin D, Hawkins A R and Schmidt H 2007 Atomic spectroscopy on a chip *Nat. Photon.* **1** 331–5
[23] Ritter R, Gruhler N, Pernice W, Kübler H, Pfau T, Löw R and Pfau T 2015 Atomic vapor spectroscopy in integrated photonic structures *Appl. Phys. Lett.* **107** 041101
[24] Aljunid S A, Chan E A, Adamo G, Ducloy M, Wilkowski D and Zheludev N I 2016 Atomic response in the near-field of nanostructured plasmonic metamaterial *Nano Lett.* **16** 3137–41
[25] Talker E, Arora P, Barash Y, Stern L and Levy U 2018 Plasmonic enhanced EIT and velocity selective optical pumping measurements with atomic vapor *ACS Photonics* **5** 2609–16
[26] Kitching J 2018 Chip-scale atomic devices *Appl. Phys. Rev.* **5** 1–38
[27] Venkataraman V, Saha K, Londero P and Gaeta A L 2011 Few-photon all-optical modulation in a photonic band-gap fiber *Phys. Rev. Lett.* **107** 193902
[28] Schwindt P D D, Knappe S, Shah V, Hollberg L, Kitching J, Liew L and Moreland J 2004 Chip-scale atomic magnetometer *Appl. Phys. Lett.* **85** 6409–11
[29] Arnold D, Siegel S, Grisanti E, Wrachtrup J and Gerhardt I 2017 A rubidium Mx-magnetometer for measurements on solid-state spins *Rev. Sci. Instrum.* **88** 023103
[30] Weller L, Kleinbach K S, Zentile M A, Knappe S, Hughes I G and Adams C S 2012 Optical isolator using an atomic vapor in the hyperfine Paschen–Back regime *Opt. Lett.* **37** 3405–7
[31] Talker E, Arora P, Dikopoltsev M and Levy U 2019 Realization of optical isolator at room temperature in miniaturized vapor cell using light-induced atomic desorption *CLEO 2019* vol 1 (San Jose, CA: OSA)
[32] Perez M A, Nguyen U, Knappe S, Donley E, Kitching J and Shkel A M 2008 Rubidium vapor cell with integrated nonmetallic multilayer reflectors *IEEE Micro Electro Mechanical Systems* pp 790–3
[33] Vanier J, Audoin C and Sud P 1989 *The Quantum Physics of Atomic Frequency Standards Volume 1* vol 1 (Bristol: IOP Publishing)
[34] Auznish M and Ferber R 2005 *Optical Polarization of Molecules* (*Cambridge Monographs on Atomic, Molecular and Chemical Physics) (Ed.),*) ed A Dalgarno *et al* (Cambridge: Cambridge University Press)